A Fully Digital Background Calibration of Timing Skew in Undersampling TI-ADC

Han Le Duc*, Chadi Jabbour*, Patricia Desgreys*, Olivier Jamin†, and Van Tam Nguyen*‡
*Institut Mines-Télécom, Télécom ParisTech, CNRS/LTCI, 46 Rue Barrault, 75013 Paris, France
†NXP Semiconductors, 2 Esplanade Anton Phillips, 14000 Caen, France
‡Department of EECS, University of California at Berkeley, California, 94720, USA
Email: han.le-duc@telecom-paristech.fr

***Abstract*—This paper proposes a fully digital calibration of timing mismatch for undersampling Time Interleaved Analog-to-Digital Converter (TI-ADC) employed in Software Defined Radio (SDR) receivers. The proposed calibration scheme employs an ideal differentiator filter, a Hilbert transform filter and a scaling factor to compute the derivative of the input in any Nyquist Band (NB). The efficiency of the proposed technique is shown using a four-channel undersampling 60 dB SNR TI-ADC clocked at 2.7 GHz. Monte Carlo simulations show SNDR and SFDR improvements of respectively, 18 dB and 21 dB over the first three NBs.**

I. Introduction

The need for low power, low implementation cost, high resolution and especially very high speed data conversion has created very rich research activity for TI-ADCs for the last decade. Time-interleaved ADCs, which are formed by several slow but accurate ADCs in parallel, is not only a mean of increasing the conversion speed, but also can relax their power-speed tradeoffs, reduce their metastability error rate while increasing the input capacitance [1]. However, offset, gain and timing mismatches among the sub-ADCs reduce the achievable linearity and significantly degrade the performance of TI-ADC [2]. Among these aforementioned errors, the sample-time error is the most critical, due to its frequency depending detection. The impact of timing skew rises with input frequency. For these reasons, we will mainly focus in this paper on the timing mismatches for the input signals located in any Nyquist band.

An all-digital background calibration technique to mitigate the errors caused by timing mismatch is preferred in order to take the advantages of technology scaling, the flexibility of digital circuits and the ease of portability from one technology node to the following. Most of the existing digital sample-time error correction mechanisms work only for bandlimited input signal at the first NB. Such methods are either based on digital fractional delay filter as reported in [3]–[6] or canceling structure formed by derivative filter and real modulators [7]–[9]. Most of them are not able to directly perform timing skew calibration for undersampling TI-ADCs, which are however an interesting solution to remove the last mixing stages for all-digital receivers such as SDR receivers. The work presented in [4] deals with the calibration of sample-time errors in undersampling TI-ADC, but under the assumption of narrow-band signals and for only two channels. The calibration scheme presented in [10] copes directly with timing skews in the undersampling TI-ADCs, but at the price of an additional channel. Another approach reported in [3] requires a pilot input signal and adds constraints on the useful signal bandwidth.

This paper extends the work of J. Matsuno *et al.* presented in [9] to all NBs with relaxed constraints on input. The paper is organized as follows. Section II describes the system model of TI-ADC and the error signal due to timing skews as a function of input's derivative. Section III is dedicated to the description of limitations of the correction circuit using a fixed derivative filter for input outside the first NB. After that proposed digital background calibration scheme for the input signals in any NB is presented. Simulation results and conclusion are presented in Section IV and V, respectively.

II. System Model

Figure 1 shows a model of a M-channel time-interleaved ADC without quantization noise. The analog input signal $x(t)$ is fed into M-channel frequency responses, and then downsampled with the same sampling rate of $\frac{f_s}{M}$. The overall sampling frequency of TI-ADC f_s is M times higher than that of individual ADCs. The downsampled outputs $z_m[n]$ are time-aligned by upsamplers and delay elements $z^{-m}, m = 0, 1, \cdots, M-1$. The sum of channel outputs is the digital output of the TI-ADC. In this section, offset and gain mismatches are assumed to be calibrated. The sample-time error values are defined relatively to the average value. Thus, the sum of timing mismatch of individual channel is equal to zero. The channel response can then be expressed by:

$$H_m(j\omega) = e^{j\omega(m+\tau_m)}, m = 0, 1, \cdots, M-1, \tag{1}$$

where τ_m is the relative time offset of the m-channel that is the ratio between deterministic absolute time offset and sampling period T_s. In practice, the absolute time offsets are typically small compared to the sampling period T_s [5]. By assuming a bandlimited input signal

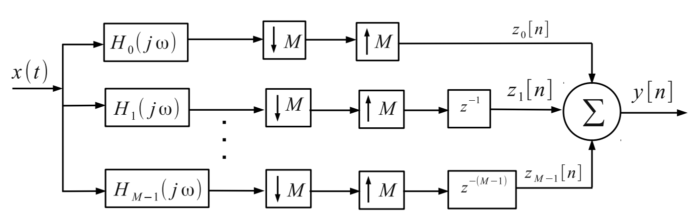

Fig. 1: Model of M-channel TI-ADC

$X(j\Omega)$, i.e., $X(j\Omega) = 0$ for $|\Omega T_s| \geq \pi, \omega = \Omega T_s$, the relationship between input and output of TI-ADC can be written by [7]:

$$Y(j\omega) = \sum_{k=0}^{M-1} \alpha_k \left(j(\omega - k\frac{2\pi}{M})\right) X\left(j(\omega - k\frac{2\pi}{M})\right), \tag{2}$$

with

$$\alpha_k\,(j\omega) = \frac{1}{M}\sum_{m=0}^{M-1} H_m(j\omega)e^{-j\omega m}e^{-jk\frac{2\pi}{M}m}. \tag{3}$$

By exploiting the Taylor's series approximation and neglecting the high orders, i.e., $e^{j\omega\tau_m} \approx 1 + j\omega\tau_m$, with $\tau_m \ll 1$, and then substituting (1), (3) into (2), TI-ADC output spectrum can be written by:

$$Y(j\omega) \approx X(j\omega) + \sum_{k=0}^{M-1} \tau_k Z_k^{'}(j\omega), \tag{4}$$

$$Z_k^{'}(j\omega) = \Bigg[\frac{1}{M} \sum_{m=1}^{M-1} e^{-jk\frac{2\pi}{M}m} \times H_d\left(j(\omega - m\frac{2\pi}{M})\right) X\left(j(\omega - m\frac{2\pi}{M})\right) \Bigg], \tag{5}$$

and

$$H_d(j\omega) = j\omega. \tag{6}$$

$H_d(j\omega)$ is the frequency response of an ideal discrete-time differentiator [11]. Obviously, the first term in (4) is the wanted signal, while the second term is the error due to timing mismatches. This error is the sum of complex constituent signals $Z_k^{'}(j\omega)$ that are the derivative of input signal, whose frequency is shifted, and then modulated by the different complex modulators of $e^{-jk\frac{2\pi}{M}m}$. These signals are uncorrelated with the input. They will be referred to as Pseudo Aliasing (PA) signals [9].

III. Digital Calibration of timing skew for any Nyquist Band

A. Limitation of the correction circuit using a fixed differentiator filter for input outside the first NB

Based on (5), the authors in [7]–[9] built a digitally efficient correction circuit of sample-time errors which is formed by real modulators and a fixed discrete-time derivative filter with frequency response written by (6) for the first NB. To obtain the causal and realizable FIR filter in practice, the infinite impulse response $h_d[n]$ that is the inverse Discrete-time Fourier Transform (DFT) of $H_d(j\omega)$, can be truncated, windowed and shifted. However, only one differentiator filter in the correction circuit limits the efficiency of the correction technique to the first NB. In Fig. 2, the undersampling TI-ADC converters with sampling frequency satisfying the Nyquist criterion, fold the original spectrum of Bandpass (BP) signal back to base-band. According to BP sampling theory discussed in [11],

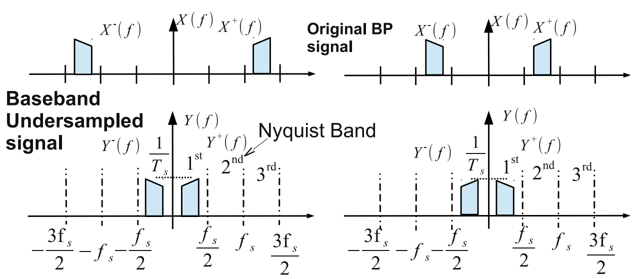

(a) The odd-order BP input signal (b) The even-order BP input signal

Fig. 2: Examples of undersampling process.

the baseband spectrum of undersampled signal when input signal is in the odd-order NB, has the same shape as the original spectrum as shown in Fig. 2(a). There is a flip in the frequency spectrum in baseband for the even-order NB input signal in Fig. 2(b). As a result, the derivative of the output baseband signal is not identical to the derivative of sampled version of original BP signal that is required to correct the sample-time errors. This leads to the common limitation to employ the correction technique reported previously in [7]–[9] for input signal outside the first NB. The proposed technique in this paper overcomes this limitation. It will be elaborated in the next section.

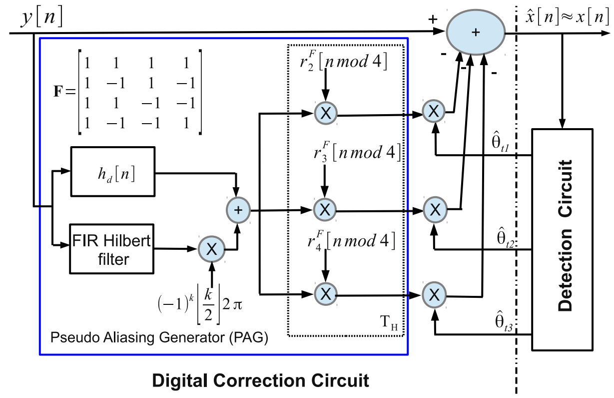

Fig. 3: The proposed technique for input occupied at k-th NB for M=4 channel undersampling TI-ADC.

B. Proposed calibration for any Nyquist Band

To formulate the first-order derivative of original BP sampling signal in even- or odd- Nyquist bands, the input signal is considered as sum of two complex signals of $x^+(t)$ and $x^-(t)$ having the positive and negative frequency spectrum, $X^+(f)$ and $X^-(f)$, respectively. Similarly, the TI-ADC output at baseband can be written by $Y(f) = Y^+(f) + Y^-(f)$, see Fig. 2. Intuitively, the spectrum of original BP signal at frequency f is translated to that of baseband output signal at $f \pm f_s$. Let us take for example the third-order undersampling process for the first analysis. The relationship between spectrum of a real BP signal and baseband output can be expressed by:

$$\begin{aligned} X(f) &= X^-(f) + X^+(f) \\ &= T_s Y^+(f - f_s) + T_s Y^-(f + f_s). \end{aligned} \tag{7}$$

After taking the inverse DFT of (7), the original BP signal in time domain can be expressed by:

$$x(t) = T_s y^+(t) e^{j2\pi f_s t} + T_s y^-(t) e^{-j2\pi f_s t}. \tag{8}$$

In the time domain, the relationship between the lowpass signals of $y^+(t)$ and $y^-(t)$ and $y(t)$ is provided by [11] as follows.

$$\begin{aligned} 2y^+(t) &= y(t) + j\hat{y}(t), \\ 2y^-(t) &= y(t) - j\hat{y}(t), \end{aligned} \tag{9}$$

where $\hat{y}(t)$ is the Hilbert transform of $y(t)$. After replacing (9) into (8), the original BP signal can be expressed by:

$$x(t) = T_s y(t) cos(2\pi f_s t) - T_s \hat{y}(t) sin(2\pi f_s t). \tag{10}$$

By differentiating and sampling this original BP signal, the relationship between the first-order derivative of the original BP signal, the derivative and Hilbert transform of undersampled signal can be expressed by:

$$x'[n] = y'[n] - 2\pi\hat{y}[n]. \tag{11}$$

With the same procedure, the first-order derivative of the BP signal located in the second NB is derived by:

$$x'[n] = y'[n] + 2\pi\hat{y}[n]. \tag{12}$$

The general first-order derivative of BP signal located at k-th NB can be expressed by:

$$x'[n] = y'[n] + (-1)^k \left\lfloor \frac{k}{2} \right\rfloor 2\pi\hat{y}[n], \tag{13}$$

where $\lfloor x \rfloor$ is a nearest integer less than or equal to x. From (13), the proposed filter block to calculate the derivative of the BP input signal is constructed by a derivative filter, a Hilbert transform filter and scale factor $(-1)^k \left\lfloor \frac{k}{2} \right\rfloor 2\pi$; the overall calibration structure of the timing skew for four-channel undersampling TI-ADCs is introduced in Fig. 3. In general, this calibration architecture can be easily extended to M-channel.

1) Digital Correction Circuit: The digital correction circuit consists of multipliers and the Pseudo Aliasing Generator (PAG) formed by the proposed filter block and Hadamard modulation vectors $r_i^{\mathbf{F}}[n \ mod \ M]$ that are the cyclic repetition of the i-th row of a M-th order Hadamard modulation matrix $\mathbf{F}$, $i = 2, \ldots, M$, labeled in Fig. 3. The mod is a modular arithmetic. The PA signals at PAG outputs are multiplied with the time offset coefficients $\hat{\theta}_{tl}, \ l = i-1$, which are functions of timing skew of individual sub-ADC to create the global error signal. Finally, subtracting the obtained error signal from TI-ADC output with sample-times errors produces the compensated signal.

2) Digital Detection Circuit: The cross-correlation-based sample-time error detection scheme presented in [4], [6], [9], [12], is applied in our proposed solution. A block diagram of the digital detection circuit is shown in Fig. 4 which encompasses a PAG, a correlator and an optional notch filter. The PAG block is the same as that of the digital correction circuit. The correlator in [9] computes the cross correlation between the compensated signal $\hat{x}[n]$ and PA signals $\hat{x}'_{el}[n]$ that are outputs of the PAG in the detection circuit. The compensated signal still has the residual aliasing signals during the timing mismatch coefficient convergence. Thus, the feedback loops make the correlation close to zero. Correlator output then converges to the expected values of timing mismatch coefficients. An adaptive learning algorithm to update the timing mismatch coefficients can be driven by:

$$\hat{\theta}_{tl}[n+1] = \hat{\theta}_{tl}[n] + \mu_t(\hat{x}[n]\hat{x}'_{el}[n]), \qquad (14)$$

where $l = 1, 2, \cdots, M-1$ and μ_t is the adaptation step size. There

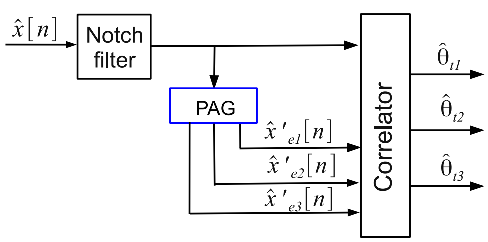

Fig. 4: Digital Detection Circuit of timing skew for four-channel undersampling TI-ADC.

are two common limitations for this detection technique. Firstly, the detection is inaccurate if the input signal contains frequency components at $l\frac{\pi}{M}, l = 1, 2, \cdots, M-1$. A notch filter is used in front of detector to mitigate the amplitudes at these notch frequencies as illustrated in Fig. 4. Secondly, the detection technique does not converge as well as the input contains at least two frequency components satisfying $\omega_a \pm \omega_b = l\frac{2\pi}{M}, l = 1, 2, \cdots, M-1$. The output of the correlator will converge to non zero DC value even if there are no timing mismatches among channels [12].

IV. Simulation Results

To verify the efficiency of the proposed technique, simulations were carried out on an undersampling four-channel 60 dB SNR TI-ADC clocked at $f_s = 2.7$ GHz. The quantization is performed over 11 bit. Both the ideal differentiator and Hilbert filter have 31-taps. The coefficients of FIR filters are obtained by multiplying the exact coefficients with a Blackman window.

Since offset and gain mismatches are static errors, a classical calibration scheme applied efficiently for the input in the first NB, is employed in addition to the proposed technique in order to address all

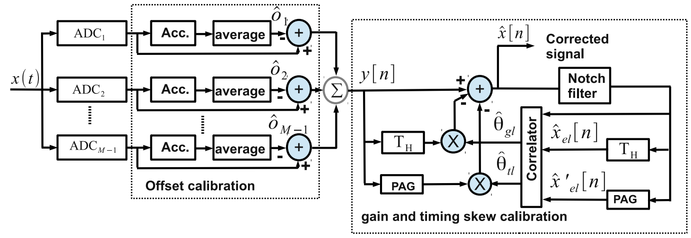

Fig. 5: Block diagram of the adaptive calibration system.

mismatches. An overall calibration architecture for offset, gain and timing errors is drawn in Fig. 5. In the offset calibration block, the offset values are estimated by accumulation denoted by **Acc.**, and average of N_s samples of each sub-ADC: $\hat{o}_i = \sum_{n=0}^{N_s} z_i[n], i = 0, \ldots, M-1$. These estimates of the offset errors are subtracted from the channel output. Once the offset calibration is done, gain and sample-time mismatches are estimated and corrected at once. Since gain errors are frequency independent, the calibration for gain mismatches proposed in [9] is also applied herein for the input signals located in any NB. Block $\mathbf{T_H}$ is the Hadamard transform which was described in Fig. 3 of Section III. The gain mismatch coefficients of $\hat{\theta}_{gl}[n], l = 1, \ldots, M-1$, are updated by the learning equations:

$$\hat{\theta}_{gl}[n+1] = \hat{\theta}_{gl}[n] + \mu_g(\hat{x}[n]\hat{x}_{el}[n]), \qquad (15)$$

where μ_g is the adaptation step size for the gain mismatches. We model simulation with realistic values of mismatch errors from experience. This gives offset values of $[0, 0.0158, -0.0014, -0.0229]$, gain mismatch values of $[0, 0.0171, 0.0331, -0.0009]$, and timing skews of $[0, -1.3055, -1.3879, 0.2378]$ps. Adaptation step sizes of μ_g, μ_t are chosen respectively $2^{-13}, 2^{-18}$ based on simulation in order to achieve a good compromise between the convergence speed and the parameter estimation precision [13]. The Number of FFT (NFFT) points used to plot the spectrum is 2^{18} samples. Simulations are performed with single-tone input signal located in the second Nyquist band at $f_{in} = 0.41 \times f_s + \frac{f_s}{2}$.

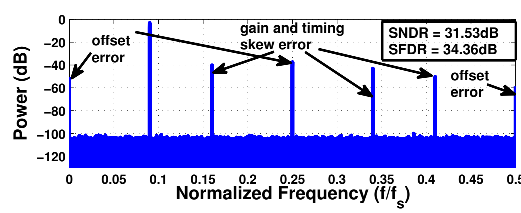

(a) before calibration

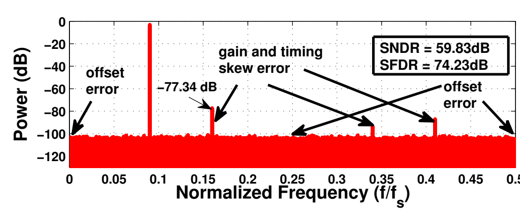

(b) after calibration

Fig. 6: Measured output spectrum for $f_{in} = 0.41 \times f_s + \frac{f_s}{2}$ (in second Nyquist band): (a) before, and (b) after calibration. (Due to undersampling TI-ADC, f_{in} maps to $0.09 \times f_s$ in baseband).

Figure 6 shows the output spectra before and after calibration. The SFDR is improved by almost 40 dB. The SNDR value after calibration is 60 dB which is equal to its value in the no-mismatch case. The right-hand side of Fig. 7 shows the divergence of the sample-time error correction loop performed by the calibration described in [9], whereas in the proposed calibration, the sample-time error coefficient estimates converge to their expected values after 55K-samples (or after 20μs), see in the left-hand side of Fig. 7.

Monte Carlo simulations were carried out as well to evaluate the performance of the proposed calibration. All errors are Gaussian with zero mean and standard deviation of 2 ps for timing skew and 0.02% for offset and gain mismatches. NFFT points is 2^{18}. (μ_g, μ_t) are chosen equal to $(2^{-14}, 2^{-15}), (2^{-16}, 2^{-15})$, and $(2^{-15}, 2^{-16})$ with respect to the first three NBs. Figures 8 and 9 show the histograms of SNDR and SFDR before and after calibration with one tone input inside the k-th NB at $f_{in_k} = 0.405 \times f_s + (k-1)\frac{f_s}{2},\ k = 1, 2, 3$. The mean ($\mu$) and standard deviation (σ) of SNDR and SFDR are shown in the figures. As can be seen, the SNDR and SFDR without calibration decrease when the NB order increases. This is due to the higher impact of the timing skew with the input frequency increase [1]. After calibration, the SNDR and SFDR remain smaller for higher NBs. As a matter of fact, in (5), the PA signals are generated from the input signal $x[n]$. However, since it is not available, the PA signals are generated using the TI-ADC output $y[n]$ as illustrated in Fig. 3. This approximation becomes less accurate when the input frequency is increased because the distortion level rises. Nevertheless, the achieved SFDR improvement remains significant which proves the efficiency and interest of the proposed technique.

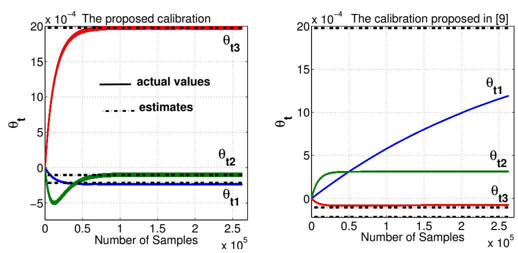

Fig. 7: Convergence of the gain and timing mismatch coefficients of θ_t with single-tone input signal in 2nd NB for the proposed calibration (left-hand side) and the calibration proposed in [9] (right-hand side).

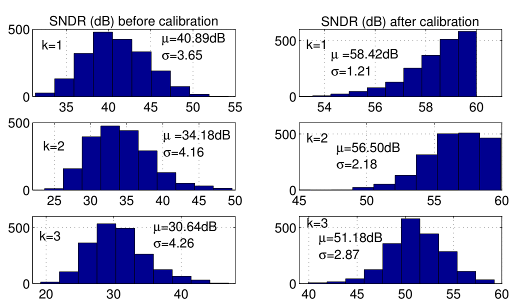

Fig. 8: Histograms of SNDR before and after calibration in the first three NBs: $k = 1, 2, 3$.

V. Conclusion

This paper proposes a digital background calibration technique of sample-time error for undersampling TI-ADCs with input signals at any NB. The technique does not require a pilot input nor additional reference channel. It just requires a differentiator, a FIR Hilbert filter and a scaling factor to determine the first-order derivative of the input in different NBs. Simulations have shown the efficiency of the proposed calibration which leads to SNDR and SFDR improvement of 18 dB and 21 dB respectively for four-channel undersampling 60 dB SNR TI-ADC clocked at 2.7 GHz over the first three NBs.

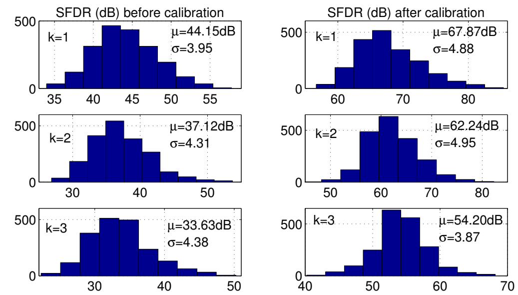

Fig. 9: Histograms of SFDR before and after calibration in the first three NBs: $k = 1, 2, 3$.

Acknowledgments

The authors would like to thank the European Catrene AppsGate project for supporting this work.

References

[1] B. Razavi, "Design considerations for interleaved adcs," *Solid-State Circuits, IEEE Journal of*, vol. 48, no. 8, pp. 1806–1817, 2013.

[2] C. Vogel, "The Impact of Combined Channel Mismatch Effects in Time-Interleaved ADCs," *IEEE Transactions on Instrumentation and Measurement*, vol. 54, no. 1, Feb. 2005.

[3] E. Venosa, F. J. Harris, and F. A. N. Palmieri, *Software Radio, sampling rate selection, design and Synchronization*. Springer New York Dordrecht Heidelberg London, 2012.

[4] S. Jamal, D. Fu, M. Singh, P. Hurst, and S. Lewis, "Calibration of sample-time error in a two-channel time-interleaved analog-to-digital converter," *Circuits and Systems I: Regular Papers, IEEE Transactions on*, vol. 52, no. 4, pp. 822–822, 2005.

[5] S. Huang and B. Levy, "Adaptive blind calibration of timing offset and gain mismatch for two-channel time-interleaved ADCs," *IEEE Transactions on Circuits and Systems I: Regular Papers*, vol. 53, no. 6, pp. 1278–1288, Jun. 2006.

[6] C. H. Law, P. Hurst, and S. Lewis, "A four-channel time-interleaved adc with digital calibration of interchannel timing and memory errors," *Solid-State Circuits, IEEE Journal of*, vol. 45, no. 10, pp. 2091–2103, 2010.

[7] C. Vogel, S. Saleem, and S. Mendel, "Adaptive blind compensation of gain and timing mismatches in m-channel time-interleaved adcs," in *Electronics, Circuits and Systems, 2008. ICECS 2008. 15th IEEE International Conference on*, 2008, pp. 49–52.

[8] V. Divi and G. W. Wornell, "Blind calibration of timing skew in time-interleaved analog-to-digital converters," *Selected Topics in Signal Processing, IEEE Journal of*, vol. 3, no. 3, pp. 509–522, 2009.

[9] J. Matsuno, T. Yamaji, M. Furuta, and T. Itakura, "All-digital background calibration technique for time-interleaved adc using pseudo aliasing signal," *Circuits and Systems I: Regular Papers, IEEE Transactions on*, vol. 60, no. 5, pp. 1113–1121, 2013.

[10] F. Centurelli, P. Monsurro, and A. Trifiletti, "Efficient digital background calibration of time-interleaved pipeline analog-to-digital converters," *Circuits and Systems I: Regular Papers, IEEE Transactions on*, vol. 59, no. 7, pp. 1373–1383, 2012.

[11] J. G. Proakis and D. G. Manolakis, *Digital Signal Processing: Principles, Algorithms and Applications.* Upper Saddle River, New Jersey, 2007.

[12] D. Camarero, K. Ben Kalaia, J.-F. Naviner, and P. Loumeau, "Mixed-signal clock-skew calibration technique for time-interleaved adcs," *Circuits and Systems I: Regular Papers, IEEE Transactions on*, vol. 55, no. 11, pp. 3676–3687, 2008.

[13] P. Diniz, *Adaptive Filtering: Algorithms and Practical Implementation*, ser. Kluwer international series in engineering and computer science. Springer, 2008.